OPEN ACCESS
Journal of Innovative Optical Health Sciences
Vol. 14, No. 1 (2021) 2140010 (12 pages)

DOI: 10.1142/S1793545821400101

World Scientific
www.worldscientific.com

Refractive index characteristics of edible oils based on spectrometry and effects of oil dispersion on OCT

ShiJun Xu and XiaoKang Li*
School of Science
Xi'an Technological University
Xi'an 710021, P. R. China
**547299061@qq.com*

Received 29 September 2020
Accepted 28 December 2020
Published 27 January 2021

It is necessary to investigate the wavelength-dependent variation rules of the refractive index of edible oils so as to explore the specificity of the dispersion in light propagation, imaging, and interference processes among different types of edible oil products. In this study, by deriving the refractive index equations of the double glass sheet holding device and oil, the reflectance spectra of three different types of oil samples, namely, peanut oil, colza oil, and kitchen waste oil, were measured via a spectrometer. Furthermore, the refractive index model of these different types of oil samples was investigated. Additionally, based on the oil dispersion characteristics, the dispersion of oil in optical coherence tomography (OCT) was compensated via deconvolution. In the wavelength range of $\lambda \in (380, 1500)$ nm, the analytical expressions of the double glass sheet holding device and oils are featured by practical reliability. The refractive indexes of three different types of oils $n \in (1.38, 1.52)$ show normal dispersion characteristics. The Cauchy coefficient matrix of the oil refractive index can be used for oil identification; in particular, the healthy oil and waste oil differ significantly in terms of the Cauchy coefficient matrix in the infrared band. Oil dispersion has almost no influence on the phase spectra of oils but can enhance their amplitude spectra. The dispersion mismatch can be eliminated by calculating the convolution kernel. The envelope broadening factors of OCT interference signals of oil products are 0.84, 0.64, and 0.91, respectively. According to the present research results, the refractive index model of oil can effectively remove the influence of the holding device. The refractive indexes of three different types of oil samples show similar wavelength-dependent variation characteristics, which confirms the existence of many correlated components in these oil samples. The established refractive index model of oil in a wide spectral range, from the ultraviolet to the infrared band, can be adequately employed for identifying different types of oils. The numerical dispersion compensation based on the established refractive index model can enhance the axial resolution in OCT imaging.

Keywords: Biological optics; refractive index; spectrometer; edible oil; dispersion; OCT.

*Corresponding author.

1. Introduction

Safety detection is particularly important for edible oils.[1] Currently, common techniques for edible oils and the finished products mainly include conventional physical and chemical detection, chromatography, nuclear magnetic resonance identification, and spectroscopy. However, due to the lack of effective detection systems and standards, researchers have gained insufficient knowledge regarding oil dispersion characteristics and related detection using the existing optical methods, such as Fourier transform-infrared (FT-IR) spectroscopy,[2] biomass spectrometry,[3] low-field NMR,[4] and Terahertz spectroscopy.[5]

Researchers generally use the Cauchy equation for accurately characterizing the dispersion relation of biological material.[6] With regard to edible oils, only Chengchao *et al.* from the Harbin Institute of Technology performed the characterization of wavelength-dependent refractive index variation rules of both colza oil and peanut oil using the Cauchy equation via double light path transmission.[6,7] According to their results, the refractive index of colza oil at 632.8 nm was 1.5197; however, they did not examine waste oil, and different types of oils exhibit no specificity. Zhang *et al.*[8] from the University of Shanghai for Science and Technology employed light interference fast measurements on different oils at room temperature, with a wavelength of 632.8 nm. Through these measurements, the refractive indexes of the Luhua 5S first-grade pressing peanut oil and the Duoli highly flavored colza oil were found to be 1.4709 and 1.4718, respectively. Overall, the measured refractive indexes of different types of oils in previous studies were poor in regularity and restricted in the narrow visible wavelength range, thereby providing less support for oil identification.

In this study, the reflectance spectra of colza oil, peanut oil, and kitchen waste oil were measured using a spectrometer to investigate the variation characteristics of the oil refractive index with wavelength. Moreover, the dispersion characteristics of various types of edible oils were accurately characterized via the Cauchy equation. In contrast with the double light path transmission method, the present method exhibits high precision and is more convenient in operation.[6] In addition, the Cauchy refractive index matrices of different types of oils show a significant difference. On this basis, the dispersion compensation of oil during the imaging process was investigated by means of optical coherence tomography (OCT), and the dispersion mismatch of the sample was eliminated by calculating the convolution kernel, thereby effectively enhancing the axial resolution of OCT.

2. Experiment

2.1. *Experimental samples and holding device*

In this study, three different types of edible oils, namely, colza oil (nongenetically modified organism (non-GMO) first-grade colza oil from Fulinmen Company), peanut oil (5S pressing first-grade peanut oil from Luhua Company), and kitchen waste oil (Luhua peanut oil that was fried several times), as shown in Fig. 1, were measured. The holding device consisted of two layers of microscope slides with a thickness of 1.2 mm. The two slides were glued in parallel with a spacing of 0.0615 mm, as shown in Fig. 2.

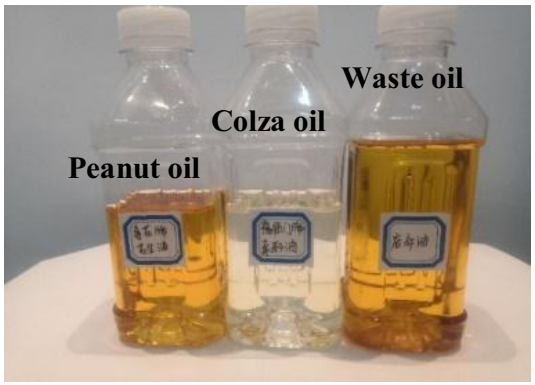

Fig. 1. Experimental samples.

Fig. 2. Double glass sheet holding device.

2.2. *Experimental instrument*

The spectra were measured using a LAMBDA950 ultraviolet-visible-infrared spectrometer manufactured by the PERKINELMER Company with a wavelength range of 175–3300 nm (380–1500 nm was used in this study). In particular, the bandwidth of the resolution is 0.05 nm, the wavelength precisions are ±0.08 nm and 0.30 nm in UV/VIS and NIR ranges, respectively, the wavelength repeatability is below 0.005 nm, and the baseline flatness is below 0.0008 A. A deuterium lamp serves as the light source in the wavelength range of 175–319.2 nm, while a halogen lamp serves as the light source in the wavelength range of 319.2–3300 nm. All optical devices adopt a total reflection circuit arrangement so as to effectively eliminate wavelength discrimination. A double-beam integrating sphere was arranged in the instrument, whose inner diameter and wavelength range are 150 mm and 200–2500 nm, respectively.

2.3. *Experimental methods*

First, different oil samples (colza oil, peanut oil, and kitchen waste oil) were added to the double glass sheet holding device for quiescence. Next, in order to achieve a baseline calibration, the spectrometer was preheated for 5 min. Finally, the double glass sheet holding devices with different oil samples were placed inside the sample chamber of the spectrometer. During the whole scanning process, the light beam was kept at vertical incidence, and the reflectance spectra in the wavelength range of 380–1500 nm were selected for further analysis.

3. Holding Device and the Refractive Index Model of Oil

3.1. *Theoretical analysis of the refractive index of the double glass sheet holding device*

As shown in Fig. 2, a certain air gap was presented between two glass sheets for holding the sample. Figure 3 displays the light paths of the device.

3.1.1. *Air–glass sheet ① — sample transmission process*

n_1, n_2, and n_3 are the refractive indexes of air, the glass sheet, and the sample, respectively. The single reflectivity at interface a and the single reflectivity at

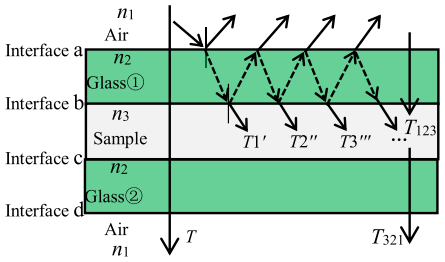

Fig. 3. Light paths of the double glass sheet device.

interface b are denoted as R_1 and R_2, respectively. T_1 and T_2 are the single transmissivities at interface a and interface b, respectively; T denotes the total transmissivity of the double glass sheet holding device measured via the spectrometer; $T1'$ denotes the transmissivity of the transmission light from interface b after passing through interface b for the first time; $T2''$ denotes the transmissivity of the transmission light from interface b after passing through interface b for the second time; $T3'''$ denotes the transmissivity of the transmission light from interface b after passing through interface b for the third time. The sum of the transmissivity when the light passes from a medium with a refractive index of n_1 to a medium with a refractive index of n_3 is denoted as T_{123}. The sum of the transmissivity when the light passes from a medium with a refractive index of n_3 to a medium with a refractive index of n_1 is denoted as T_{321}.

According to the electromagnetic wave propagation theory.[9] In the case of vertical incidence, the reflectivity can be written as

$$R_1 = \left(\frac{n_2 - n_1}{n_2 + n_1}\right)^2, \tag{1}$$

$$R_2 = \left(\frac{n_3 - n_2}{n_3 + n_2}\right)^2. \tag{2}$$

Therefore,

$$\begin{aligned} T_{123} &= T1' + T2'' + T3''' + \cdots \\ &= (1 - R_1)(1 - R_2) + (1 - R_1)(1 - R_2)R_1R_2 \\ &\quad + (1 - R_1)(1 - R_2)R_1^2R_2^2 + \cdots \\ &= (1 - R_1)(1 - R_2)\left(1 + R_1R_2 + R_1^2R_2^2 + \cdots\right) \\ &= (1 - R_1)(1 - R_2)\left(\frac{1 - (R_1R_2)^{\mathrm{n}}}{1 - R_1R_2}\right) \\ &\approx \frac{(1 - R_1)(1 - R_2)}{1 - R_1R_2} \\ &= \frac{1}{\left(\frac{1}{T_1} + \frac{1}{T_2}\right) - 1}. \end{aligned} \tag{3}$$

3.1.2. *Air–glass sheet ② — sample transmission process*

Similarly to the analysis in Sec. 3.1.1, T_{321} can be written as

$$T_{321} = \frac{1}{\left(\frac{1}{T_2} + \frac{1}{T_1}\right) - 1}. \tag{4}$$

3.1.3. *Analytic relationship between the refractive index, the transmissivity, and the reflectivity*

The upper part of the sample is composed of air and the glass sheet, while the lower part of the sample is composed of the glass sheet and air. The two glass sheets are composed of the same material. Accordingly, the absorption of light by the glass sheet and air can be neglected. According to the derivation process of Eq. (3), the following expression can be obtained:

$$\frac{1}{T} = \frac{1}{T_{123}} + \frac{1}{T_{321}} - 1. \tag{5}$$

According to Eqs. (3) and (4), the transmissivities in the two processes equal to each other, i.e., $T_{123} = T_{321}$. Equation (5) can thus be rewritten as

$$T_{123} = \frac{2T}{1+T}. \tag{6}$$

(1) *Refractive index of the glass sheet*

First, assuming that air is the sample, then $n_3 = 1$. By substituting $n_3 = 1$ into Eq. (2), it can be obtained that $R_1 = R_2$ and $T_1 = T_2$. Next, the following expression can be derived by combining Eqs. (3) and (6):

$$T_1 = \frac{4T}{1+3T}. \tag{7}$$

Both scattering and absorption of the glass sheet can be ignored since they are quite weak. Accordingly, the following expression can be derived:

$$T_1 + R_1 = 1. \tag{8}$$

By substituting Eq. (8) into Eq. (1), the following expression can be obtained:

$$n_2 = \frac{1+\sqrt{R_1}}{1-\sqrt{R_1}} = \frac{1+\sqrt{1-T_1}}{1-\sqrt{1-T_1}}. \tag{9}$$

(2) *Refractive index of the sample*

By combining Eqs. (3) and (6), the following expression can be obtained:

$$T_2 = \frac{2TT_1}{T_1 + 3TT_1 - 2T}. \tag{10}$$

By substituting Eq. (10) into Eq. (2), it can be derived that

$$n_3 = \frac{n_2(1-\sqrt{R_2})}{1+\sqrt{R_2}} = \frac{n_2(1-\sqrt{1-T_2})}{1+\sqrt{1-T_2}}. \tag{11}$$

3.2. *Experimental results of the refractive index*

The reflectivity of the double glass sheet holding device and the total reflectivity when different oil samples were placed in the holding device were measured via the spectrometer, as shown in Figs. 4 and 5, respectively.

As shown in Fig. 4, the reflectivity of the double glass sheet holding device in the wavelength range

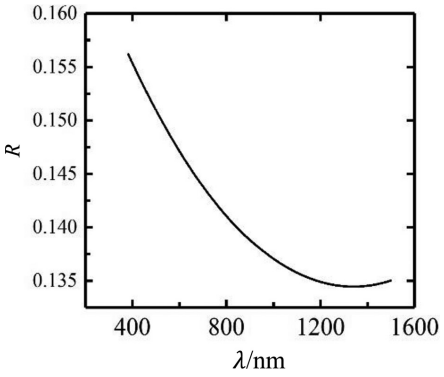

Fig. 4. Reflectivity of the double glass sheet device.

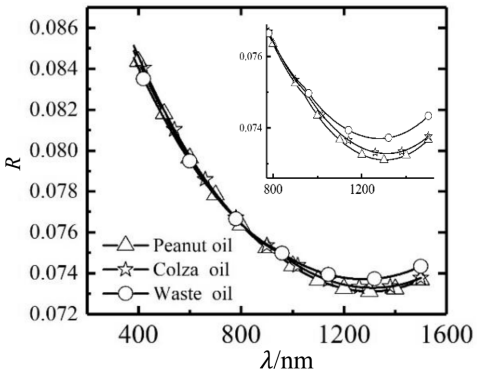

Fig. 5. Reflectivity of the three different types of oils in the double glass sheet device.

of 380–1500 nm decreases with the increase of the wavelength. It can also be observed from Fig. 5 that the reflectivity of the three different types of oil samples in the holding device drops as the wavelength increases in the range of 380–1500 nm.

The three different types of oil samples are highly similar in reflection characteristics, which indicates similar states of three samples, as well as the existence of many identical or highly correlated components. In addition, the variation of the reflectivity for the three oil samples with the wavelength also differs slightly. Moreover, the reflectivity also includes the reflection information of the holding device. The reflection characteristics of the oil sample should be extracted and the difference among different oil samples should be highlighted.

3.3. *Reflective index of the glass sheet*

By replacing T in Eq. (7) with $T = 1 - R$, the following expression can be obtained:

$$T_1 = \frac{4(1-R)}{1+3(1-R)}. \tag{12}$$

By substituting the experimental results of the refractive index into Eq. (12) and then combining Eqs. (9) and (12), the refractive index of the glass sheet n_2 can be obtained, as shown in Fig. 6.

Therefore, Eqs. (9) and (12) describe the mathematical model of the refractive index of the glass sheet in an analytical format, and Fig. 6 shows the corresponding numerical results. Evidently, the refractive index of the glass sheet decreases with the wavelength in the range of 380–1500 nm ($n_2 \in (1.4806, 1.5329)$).

Guozhong *et al.* employed the thickness transmission method for exploring the variation

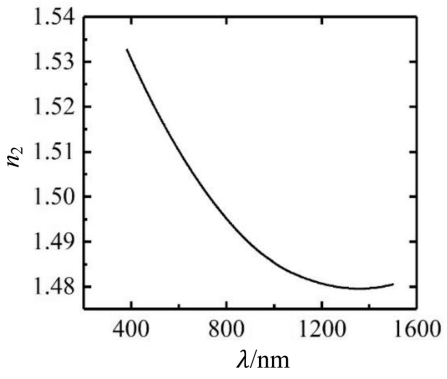

Fig. 6. Refractive index of the glass sheet.

Table 1. Two research results of the refractive index of glass sheets.

Wavelength (nm)	This article n	Literature[10] n	Relative deviation (%)
380	1.5329	1.54	0.46
400	1.5306	1.52	0.69
420	1.5283	1.53	0.11
440	1.5261	1.52	0.40
460	1.5239	1.52	0.26
480	1.5218	1.52	0.12
500	1.5197	1.51	0.64
520	1.5178	1.51	0.52
540	1.5158	1.52	0.28
560	1.5139	1.50	0.93
580	1.5121	1.51	0.14

characteristics of the refractive index of the glass sheet with the wavelength in the range of 300–600 nm.[10] In this study, the variation of the refractive index of the double glass sheet holding device with the wavelength in a broader range of 380–1500 nm was investigated via reflection. Table 1 compares the present results with the refractive index measured in Ref. 10.

It can be observed that the relative deviation of the refractive index measured in the present study with respect to the result in Ref.10 is within the range of (0.11%, 0.93%), indicating a good level of agreement. In other words, the established refractive index model based on the spectrometer is reliable. As also shown in Table 1, the present refractive index model successfully overcomes the limitation of the narrow wavelength range and shows strong regularity in a wide wavelength range of 380–1500 nm.

The relative deviation in Table 1 can be mainly attributed to the difference of the glass sheet material, experimental environment, instrument, and device precision. More specifically, the precision difference led to different significant digits of the data.

3.4. *Refractive index of oil*

By replacing T in Eq. (10) with $T = 1 - R$, it can be derived that

$$T_2 = \frac{2T_1(1-R)}{T_1 + 3T_1(1-R) - 2(1-R)}. \tag{13}$$

By substituting the measured results of the refractive index of the three different types of oil samples

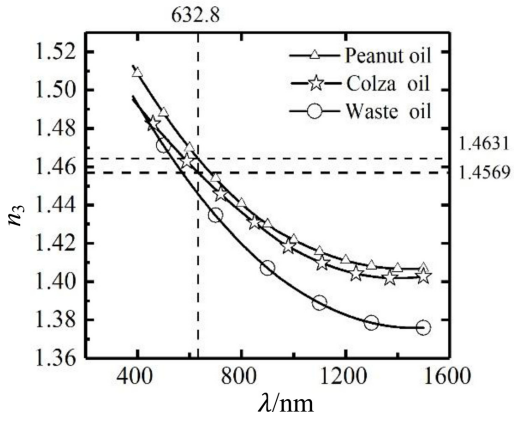

Fig. 7. Refractive index of oil.

in the holding device into Eq. (13) and then combining Eqs. (11) and (13), the refractive index of the oil (n_3) can be obtained, as shown in Fig. 7. Therefore, Eqs. (11) and (13) describe the mathematical model of the refractive index of oil in an analytical format, and Fig. 7 shows the corresponding numerical results of the refractive index.

Evidently, the refractive index of oil decreases as the wavelength increases in the range of 380–1500 mm, which is in good agreement with the conclusions in Ref. 7. This also suggests that many identical or highly correlated components exist among different types of oil samples. The reflective indexes of the three different types of oil samples exhibit significant specificity, and especially a great difference in the infrared range. The normal oil can be easily distinguished from the waste oil, which can provide theoretical foundations for establishing an oil identification system in the infrared wavelength range.

As described in Ref. 7, the holding device mainly consists of two pieces of optical glass. The variation of the refractive index of the optical glass with the wavelength was ignored in calculating the refractive index of oil, and the refractive index of the optical glass was set to an average value ($n = 1.52$); all these assumptions inevitably led to an inaccurate refractive index of oil. In this study, the characteristic function of the refractive index of the holding device with the wavelength was first investigated and then applied to the analysis of the refractive index of oil. Therefore, the conclusion regarding the refractive index of oil is more noteworthy and accurate than the results in Ref. 7.

In this study, the refractive indexes of the Luhua 5S pressing first-grade peanut oil and the Fulinmen colza oil at 632.8 nm were 1.4631 and 1.4569, respectively. The relative deviation between the present value of the Luhua first-grade peanut oil and the value using optical interference rapid measurement[8] was only 0.53%.

Table 2. Cauchy coefficients of the refractive index of the three different types of oils.

Sample	A	B	C
Peanut oil	1.38808	0.03752	−0.00299
Colza oil	1.38216	0.03850	−0.00351
Waste oil	1.35464	0.04601	−0.00395

3.5. *The Cauchy equation of the refractive index of oil*

The decreasing functions, as presented in Fig. 7, are indicative of a normal dispersion for the three types of oil samples. With regard to these bio-samples, the dispersion relation $n = n(\lambda)$ can be accurately characterized by the following Cauchy equation:

$$n = A + \frac{B}{\lambda^2} + \frac{C}{\lambda^4}, \tag{14}$$

where A, B, and C remained unchanged and are referred to as the Cauchy coefficients. By substituting the corresponding data of Fig. 7 into Eq. (14), the Cauchy coefficient matrices of the peanut oil sample, the colza oil sample, and the kitchen waste oil sample can be calculated using the method of undetermined coefficients, as shown in Table 2.

Table 2 shows the Cauchy coefficients of the refractive indexes of the different types of oil samples. The Cauchy coefficients of three different oil samples show applicable and operable distinction points. In particular, the kitchen waste oil and the healthy oil differ significantly. Therefore, an effective index system for oil identification is expected to be developed by utilizing the specificity of the Cauchy coefficients of various types of edible oils.

4. Effect of Oil Dispersion on OCT

As described in Secs. 3.4 and 3.5, oil shows distinct dispersion characteristics, and various types of oils differ in dispersion characteristics. During OCT imaging process, the dispersion characteristics of oils and the optical elements in the imaging system can cause the envelope broadening of the optical

coherent signal, thereby reducing the axial imaging resolution.[11]

4.1. *Analysis of OCT dispersion characteristics*

As shown in Fig. 8, the Michelson interferometer is the key component in OCT.[12] The light from a low-coherence source can be split into two light beams via the beam splitter, in which one beam is the reference light and the other beam is the signal detection light. The former reference beam is reflected by the reflector, then passes through the reference arm, and finally arrives at the detector. The latter detection beam is first scattered by the sample and arrives at the detector after passing through the signal arm. The signal light beam of the signal arm is interfered with the reference beam of the reference arm and finally received by the detector.[13,14]

By ignoring the DC term, the interference signal in the frequency domain received by the detector can be expressed as[15,16]

$$\begin{aligned} S(k) &= 2Re\left\{\sum_n \sqrt{I_n(k)I_r(k)}\exp\left[i\phi(k,\Delta z_n)\right]\right\} \\ &= 2Re\left\{\sum_n \sqrt{I_n(k)I_r(k)}\exp\left[i\left[k\cdot\Delta z\right]\right.\right. \\ &\quad \left.\left.+\phi(k,\Delta z_n)\right]\right\}, \end{aligned} \tag{15}$$

where $I_n(k)$ denotes the scattering intensity of the nth layer of the sample, Re is the real part, $k = 2\pi/\lambda$ denotes the wave number (WN), $I_r(k)$ denotes the light intensity returned from the reflector, $\phi(k, z_n)$ denotes the phase difference of the nth layer of the sample relative to the reference light, and ΔZ_n denotes the light path difference of the nth layer of the sample relative to the reference arm mirror. $\phi(k, z_n)$ can be written as

$$\phi(k,\Delta z_n) = \beta_n(k)\cdot\Delta z_n, \tag{16}$$

where $\beta_n(k)$ denotes the effective propagation coefficient of the nth layer of the sample. After a Taylor expansion at $\beta_n(k)$, ϕ (k,z_n) can be written as[17]

$$\begin{aligned} \phi(k,\Delta z_n) &= \left[n_n(k_0)k_0 + n_{g,n}(k_0)(k-k_0)\right. \\ &\quad + \beta_n''(k_0)\frac{(k-k_0)^2}{2} \\ &\quad \left.+ \beta_n'''(k_0)\frac{(k-k_0)^3}{6} + \cdots\right]\cdot\Delta z \\ &= n_n(k_0)k_0\cdot\Delta z + n_{g,n}(k_0)(k-k_0)\cdot\Delta z \\ &\quad + a_2\cdot(k-k_0)^2 + a_3\cdot(k-k_0)^3 + \cdots, \end{aligned} \tag{17}$$

where n_n denotes the effective refractive index of the nth layer of the sample, $n_{g,n}$ denotes the effective group refractive index of the nth layer of the sample, the third item denotes the second-order dispersion at the center frequency or the group delay dispersion per unit length, and the fourth item is referred to as the third-order dispersion per unit length. The third-order and the higher-order items are referred to as the dispersion items. According to Eq. (17), the second-order dispersion compensation coefficient a_2 can be written as

$$a_2 = \frac{\lambda^3}{2\pi}\frac{d^2n}{d\lambda^2}\cdot\Delta z. \tag{18}$$

4.2. *Deconvolution of numerical compensation for oil dispersion in OCT*

Since the interference signal received by the CCD is a real rather than complex signal, the Fourier transform of the signal may produce a complex conjugate.[18] Therefore, the interference signal should undergo a Hilbert transform in order to acquire the phase spectrum of the interference signal. The oil-depth-dependent convolution kernel can then be solved based on the oil dispersion characteristics, and the dispersion mismatch induced by the sample dispersion can be eliminated through the convolution operation. Finally, the interference signal after dispersion compensation can be

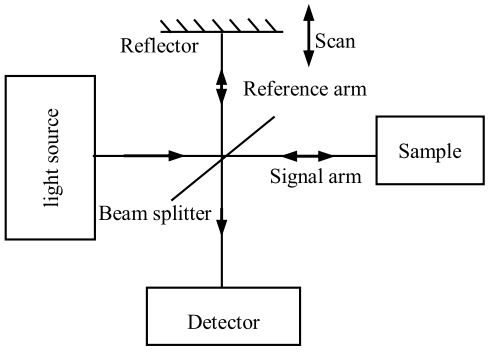

Fig. 8. Schematic diagram of the OCT imaging process.

obtained using a fast Fourier transform. The above convolution kernel can be expressed as

$$K = \mathrm{FT}^{-1}\{S(k) * \mathrm{FT}^{-1}\{\exp[-i\phi(k, \Delta z)]\}. \quad (19)$$

In the present numerical calculations, the Calisisto OCT manufactured by Thorlabs Corporation was used. The center wavelength of the imaging source and the spectral width were set to $\lambda = 930\,\mathrm{nm}$ and $\Delta\lambda = 54.52\,\mathrm{nm} = (957.26\text{–}902.74)$ nm, respectively. The dispersion characteristics of oil are described in Sec. 3.5. The oil thickness was set to $3.0 \times 10^5\,\mathrm{nm}$.

Other characteristic parameters of the OCT system are linear array InGaAs detector, A-Scan frequency is 1.2 kHz, imaging sensitivity is not less than 105 dB, axial resolution of $u_{1/2}$ in the air is $< 7.0\mu$m, radial resolution is $8\,\mu$m, maximum imaging depth is 1.7 mm, maximum resolution is 512 pixels, maximum scanning speed is 2 frames/s, visual field is $10\,\mathrm{mm} \times 10\,\mathrm{mm} \times 1.7\,\mathrm{mm}$.

4.2.1. *Phase and amplitude spectra of oils*

In the OCT system, by ignoring the DC item, the light current component produced by the light interference signal can be written as[19,20]

$$\Gamma(t) = \mathrm{real}\{E_S E_R^*\}, \quad (20)$$

where E_S and E_R denote the light fields returned via the reference arm and the sample arm, respectively; real{} denotes the real part. After the Hilbert transform, the following expression can be obtained:

$$\Gamma'(t) = \frac{1}{\pi} PV \int_{-\infty}^{+\infty} \frac{\Gamma(\tau)}{\tau - t}\, d\tau, \quad (21)$$

where PV denotes the Cauchy index of the integral. The interference signal and the Hilbert transform signal can be regarded as the real part and the imaginary part of the complex signal, respectively. Accordingly, the following expression can be derived:

$$\tilde{\Gamma}(t) = \Gamma(t) + \Gamma'(t) A(t) \exp[i\phi(t)], \quad (22)$$

where $A(t)$ and $\phi(t)$ are the amplitude and phase, respectively.

As described above, after performing the Hilbert transform and the Fourier transform on the interference signal, the frequency spectra of the peanut oil, the colza oil, and the kitchen waste oil (namely, the phase spectra and the amplitude spectra) can be obtained, as shown in Fig. 9.

Figure 9 shows the phase and amplitude spectra of the three different types of oil samples. In this figure, the N-D curves denote the signal without dispersion (corresponding to ideal conditions), while the D curves denote the signal before dispersion compensation.

By observing the results in Fig. 9, the following considerations can be made:

(1) The three types of oils show almost the same phase spectra and very similar heights in the amplitude spectra, which can be mainly attributed to similar Cauchy dispersion characteristics of the three oils and similar introduced dispersion factors.
(2) The phase curves of the three different types of oils with and without dispersion are almost coincident with each other. Since the refractive index of the oil shows no obvious change with the wavelength in the range of $\lambda \in (902.74, 957.26)$ nm, i.e., the dispersion is weak, the phase spectra with and without dispersion differ slightly.
(3) The amplitude spectra of the three different types of oils are gradually axisymmetric. By taking the right side of the symmetry axis as an example, the difference of the amplitude spectra with and without dispersion decreases with increasing frequency. Since the introduced dispersion factor imposes a decreasing effect on various high-order items, the effect of the second-order dispersion item is mainly taken into account in dispersion compensation, while the effects of the third-order and higher-order items can be ignored.
(4) By comparing the three amplitude spectra in Fig. 9, it can be easily observed that the N-D curves are always lower than the D curves, which suggests that the amplitude spectra of the interference signal drop to a certain degree without dispersion or after dispersion compensation. This reduction can be used at the expense of an increase in the axial resolution. If the effect of dispersion compensation on the OCT imaging depth is taken into account, the decrease in the amplitude spectra of the interference signal may reduce the imaging depth. Additionally, the increase of the axial resolution may increase the imaging depth. Overall, the dispersion compensation mechanism can impose bidirectional effects on the imaging depth; thus, an equilibrium state can be found.

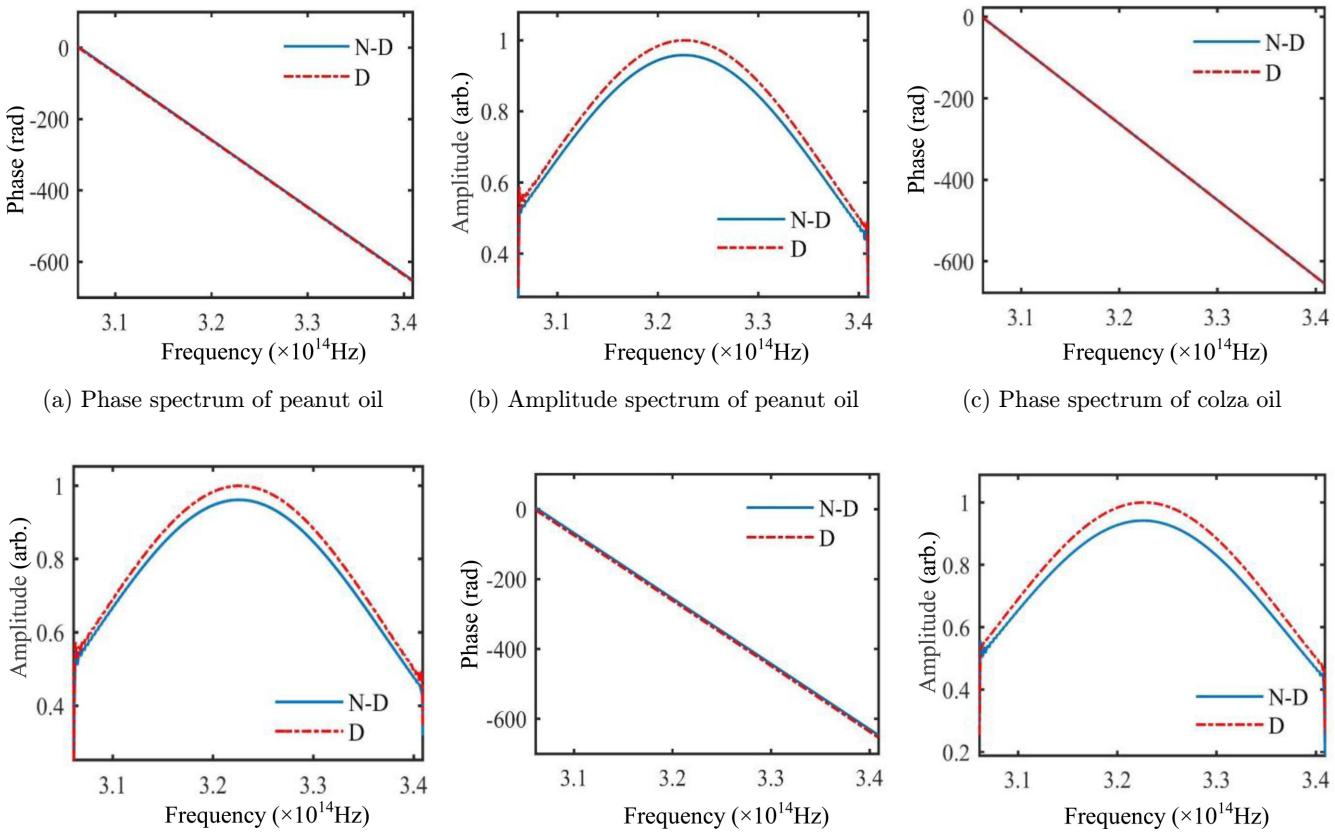

(a) Phase spectrum of peanut oil (b) Amplitude spectrum of peanut oil (c) Phase spectrum of colza oil

(d) Amplitude spectrum of colza oil (e) Phase spectrum of waste (f) Amplitude spectrum of waste oil

Fig. 9. Phase and amplitude spectra of the three oils.

4.2.2. *Comparison of the interference signals before and after dispersion compensation*

Based on the obtained dispersion characteristics of three different types of oil as described in Sec. 3.5, dispersion compensation was performed on the interference signals of different oils in OCT using the deconvolution algorithm, as shown in Fig. 10.

Figure 10 shows the envelope of interference signal before and after dispersion compensation of three edible oil samples. In this figure, the N-D curve, the D curve, and the N-D-C curve represent the signals without dispersion (in the ideal case), before, and after dispersion compensation, respectively.

In Fig. 10, the x-axis and y-axis denote the displacement of the signal arm at zero light path difference and the light intensity, respectively. The displacement L can be expressed as

$$L = d \times n_g = d \times \left(n - \lambda \frac{dn}{d\lambda}\right), \qquad (23)$$

where d denotes the thickness of the oil layer, n_g denotes the group refractive index of oil, and n denotes the refractive index of oil.

By observing the results in Fig. 10, the following considerations can be made:

(1) Assuming that the thickness of the oil is 300×10^2 nm, the characteristic displacements of the signal arm for the three different types of oils under zero light path difference are 449.6307×10^2 nm, 447.9554×10^2 nm, and 446.5344×10^2 nm, respectively, suggesting different dispersion characteristics among different oils. Additionally, since the light path equals the product of the refractive index and the distance, the characteristic displacement of the signal arm in OCT can serve as the potential index of oil identification.

(2) The interference signals of the three different types of oils before dispersion compensation show envelope broadening to varying degrees. First, the first minimum value of signal intensity in Fig. 10 is marked by the data moving mark function of

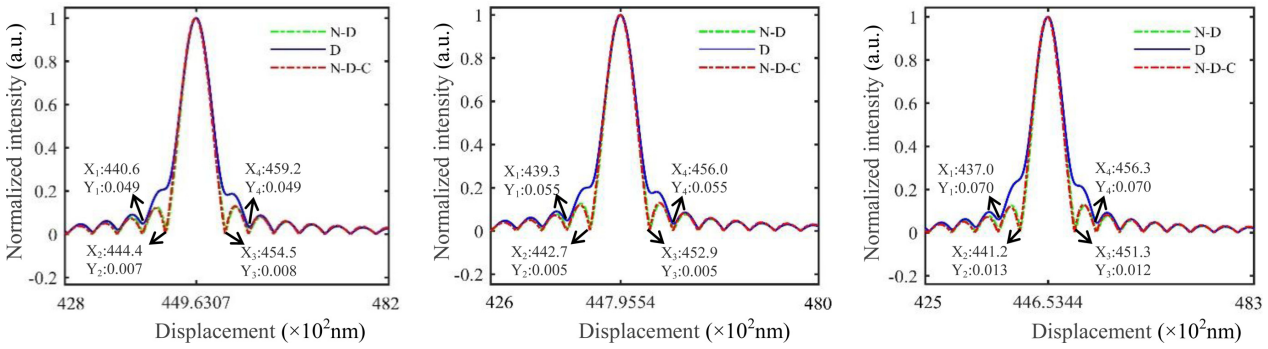

(a) Signal of peanut oil (b) Signal of colza oil (c) Signal of waste oil

Fig. 10. Envelope of interference signal before and after dispersion compensation of three edible oil samples.

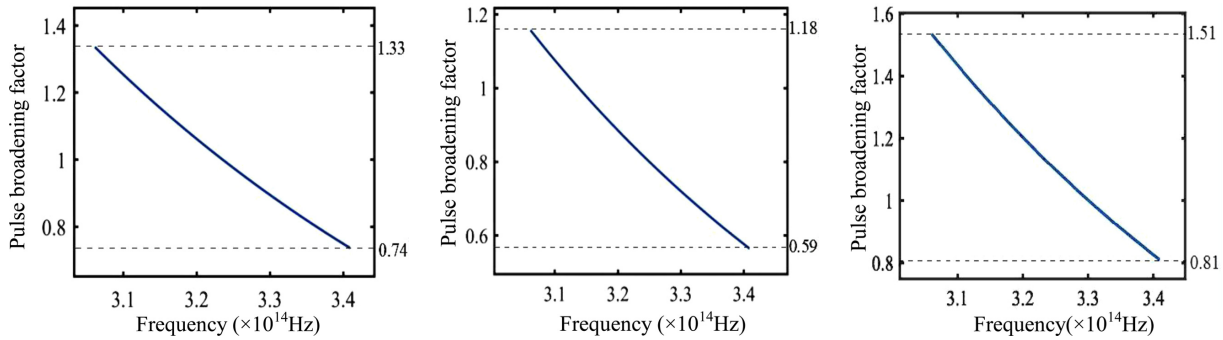

(a) Peanut oil pulse broadening (b) Colza oil pulse broadening (c) Waste oil pulse broadening

Fig. 11. Pulse broadening of three oil products.

MATLAB software, which has four points in total. Secondly, f was supposed to be the axial signal broadening factor and defined as $f = [(x_4 - x_1) - (x_3 - x_2)]/(x_3 - x_2)$. Therefore, taking peanut oil as an example, the calculated result can be expressed as $f = [(459.2 - 440.6) - (454.5 - 444.4)]/(454.5 - 444.4) = 0.84$. Similarly, the calculated f values for colza oil and waste oil are 0.64 and 0.91, respectively.

Evidently, the signal broadening significantly drops after dispersion compensation, and the signal after dispersion compensation is almost coincident with the interference signal without dispersion. Therefore, given the dispersion characteristics of the oils, the dispersion of the OCT system can be compensated via deconvolution to enhance the axial resolution.

4.2.3. *Pulse broadening induced by oil dispersion*

Since the propagation speed of light in the dispersive medium is connected with the frequency and the refractive index, the pulse signals of the light during the propagation through media with different refractive indexes show different phase delays, finally resulting in pulse broadening to different degrees. Figure 11 shows the pulse broadening results of three different types of oil samples.

It can be observed that at a frequency of 3.05×10^{14}–3.4×10^{14} Hz, the pulse broadening factors of the peanut oil sample, the colza oil sample, and the waste oil sample are in the ranges of 1.33–0.74, 1.18–0.59, and 1.51–0.81, respectively. These values are in good agreement with the above-mentioned envelope broadening factors of OCT interference signals induced by oil dispersion 0.84, 0.64, and 0.91.

5. Conclusions

The behavior of the refractive index with varying wavelength and the spectral characteristics of three different types of oil samples (peanut oil, colza oil, kitchen waste oil) are very similar, indicating the existence of many correlated components in different oils. However, the refractive index Cauchy

matrices of the three different types of oils show distinct differences. Accordingly, the mathematical model for the oil refractive index in a broad wavelength range $\lambda \in (380, 1500)\,\mathrm{nm}$ overcomes the limitations of the existing research results, such as roughness and narrow waveband, and exhibits a series of advantages, including high precision and strong general applicability. Moreover, the effect of the specific holding device can be eliminated so as to effectively highlight the specificity among different types of edible oil products. Therefore, the refractive index model and the Cauchy matrix are appropriate as effective indexes for oil identification.

Based on the dispersion characteristics of different oils (i.e., the mathematical model of the refractive index), dispersion compensation was performed on the OCT system via deconvolution, which can effectively enhance the axial imaging resolution and simultaneously reduce the amplitude spectra of the interference signal. These two results cause opposite effects on the OCT imaging depth. The present study can provide theoretical foundations for extracting different dispersion compensation parameters from different oil products in OCT experiments. Both the characteristic displacement of the signal arm in dispersion compensation and the dispersion-induced pulse broadening factors can serve as potential indexes for oil identification.

Conflict of Interest

The authors declare that there is no conflict of interest relevant to this article.

References

1. Z. Niu, M. Tong, T. Chen, "Study on food safety risk cognition based on edible oil," *Food Res. Develop.* **40**(14), 204–210 (2019) (in Chinese).
2. Z. Wu, H. Li, D. Tu, "Application of Fourier Transform Infrared (FT-IR) spectroscopy combined with chemometrics for analysis of rapeseed oil adulterated with refining and purificating waste cooking oil," *Food Anal. Methods* **8**(10), 2581–2587 (2015).
3. M. Soh, J. J. Chew, S. Liu *et al.*, "Comprehensive kinetic study on the pyrolysis and combustion behaviours of five oil palm biomass by thermogravimetric-mass spectrometry (TG-MS) analyses," *Bioenergy Res.* **12**(2), 370–387 (2019).
4. W. Zhu, X. Wang, L. Chen, "Rapid detection of peanut oil adulteration using low-field nuclear magnetic resonance and chemometrics," *Food Chem.* **216**, 268–274 (2017).
5. S. L. Zhou, S. P. Zhu, G. L. Li *et al.*, "Study on the measurement and optimization of soybean oil optical spectrum in THz range," *Spectrosc. Spect. Anal.* **36**(4), 924–928 (2016).
6. W. Chengchao, *Experimental Research and Molecular Dynamics Simulation of Optical Constants of Liquids*, Harbin Institute of Technology (2018) (in Chinese).
7. X. C. Li, J. M. Zhao, L. H. Liu *et al.*, "Optical properties of edible oils within spectral range from 300 to 2500 nm determined by double optical path length transmission method," *Appl. Opt.* **54**(13), 3886–3893 (2015).
8. H. Zhang, M. Chen, T. Tian *et al.*, "Rapid analysis of edible-oil refractive index using optical interferometry," *Optic. Instrum.* **39**(1), 1–5 (2017) (in Chinese).
9. H. A. Macleod, *Thin-Film Optical Filters*, 4th Edition, Translated by X. Degang, J. Dongfang, W. Yuye *et al.*, pp. 45–48, Science Press of China, Beijing (2016).
10. G. Wu, F. Cao, H. Qi *et al.*, "Experimental analysis on optical constants of slide glass based on transmission method," *Optic. Technique* **41**(5), 416–418 +424 (2015) (in Chinese).
11. W. J. Choi, B. Baumann, E. A. Swanson *et al.*, "Extracting and compensating dispersion mismatch in ultrahigh-resolution Fourier domain OCT imaging of the retina," *Opt. Express* **20**(22), 57–68 (2012).
12. D. Huang, E. A. Swanson, C. P. Lin *et al.*, "Optical coherence tomography," *Science* **254**(5035), 1178–1181 (1991).
13. M. Wojtkowski, V. Srinivasan, T. Ko *et al.*, "Ultrahigh-resolution, high-speed, Fourier domain optical coherence tomography and methods for dispersion compensation," *Opt. Express* **12**(11), 2404–2422 (2004).
14. D. Zhihua, C. Minghui, W. Kai *et al.*, "High-speed swept source and its applications in optical frequency-domain imaging," *Chin. J. Lasers* **36**(10), 2469–2476 (2009) (in Chinese).
15. R. Sacconi, E. Corbelli, A. Carnevali *et al.*, "Optical coherence tomography angiography in pseudophakic cystoid macular oedema compared to diabetic macular oedema: Qualitative and quantitative evaluation of retinal vasculature," *Br. J. Ophthalmol.* **102**(12), 1684–1690 (2018).
16. L. Pan, X. Wang, Z. Li *et al.*, "Depth-dependent dispersion compensation for full-depth OCT image," *Opt. Express* **25**(9), 10345 (2017).
17. L. Pan, Z. Li, X. Wang *et al.*, "Depth-dependent dispersion compensation for optical coherence

tomography," *Acta Opt. Sin.* **37**(5), 110–117 (2017) (in Chinese).
18. T. A. Al-Saeed, M. Y. Shalaby, D. A. Khalil, "Dispersion compensation in Fourier domain optical coherence tomography," *Appl. Opt.* **53**(29), 6643–6653 (2014).
19. Y.-H. Chen, Z. Ding, X.-F. Yu *et al.*, "Signal processing and image reconstruction in optical coherence tomography based on digital Hilbert transformation," *Opto-Electron. Eng.* **2006**(4), 31–34 (2006) (in Chinese).
20. L. Guozhong, Z. Zhehai, Q. Jun *et al.*, "Application of amplitude and phase registration in blood flow imaging using optical coherence tomography," *Acta Phys. Sin.* **62**(14), 556–565 (2013) (in Chinese).